JOURNAL OF GEOPHYSICAL RESEARCH, VOL. 112, D24S47, doi:10.1029/2007JD008809, 2007

Aerosols and surface UV products from Ozone Monitoring Instrument observations: An overview

Omar Torres,[1] Aapo Tanskanen,[2] Ben Veihelmann,[3] Changwoo Ahn,[4] Remco Braak,[3] Pawan K. Bhartia,[5] Pepijn Veefkind,[3] and Pieternel Levelt[3]

Received 14 April 2007; revised 11 June 2007; accepted 29 August 2007; published 29 December 2007.

[1] We present an overview of the theoretical and algorithmic aspects of the Ozone Monitoring Instrument (OMI) aerosol and surface UV algorithms. Aerosol properties are derived from two independent algorithms. The nearUV algorithm makes use of OMI observations in the 350–390 nm spectral region to retrieve information on the absorption capacity of tropospheric aerosols. OMI-derived information on aerosol absorption includes the UV Aerosol Index and absorption optical depth at 388 nm. The other algorithm makes use of the full UV-to-visible OMI spectral coverage to derive spectral aerosol extinction optical depth. OMI surface UV products include erythemally weighted daily dose as well as erythemal dose rate and spectral UV irradiances calculated for local solar noon conditions. The advantages and limitations of the current algorithms are discussed, and a brief summary of several validation and evaluation analysis carried out to assess the current level of uncertainty of these products is presented.

Citation: Torres, O., A. Tanskanen, B. Veihelmann, C. Ahn, R. Braak, P. K. Bhartia, P. Veefkind, and P. Levelt (2007), Aerosols and surface UV products from Ozone Monitoring Instrument observations: An overview, *J. Geophys. Res.*, *112*, D24S47, doi:10.1029/2007JD008809.

1. Introduction

[2] The Ozone Monitoring Instrument (OMI) is a high-resolution spectrograph that measures the upwelling radiance at the top of the atmosphere in the ultraviolet and visible (270–500 nm) regions of the solar spectrum [*Levelt et al.*, 2006]. It is one of four sensors on the Eos-Aura platform. It has a 2600 km wide swath and provides daily global coverage at a spatial resolution varying from 13 × 24 km at nadir to 28 × 150 km at the extremes of the swath. Aura is in a sun-synchronous orbit with ascending node Equator crossing time of 13:45. The Aura spacecraft is part of the A-train, which includes 3 other aerosol sensors Aqua-MODIS, Parasol, and CALIPSO. The OMI project is a joint effort by the Netherlands, Finland, and the USA.

[3] Other sensors with OMI-like hyper-spectral capabilities include European atmospheric research instruments such as the Global Ozone Monitoring Experiments (GOME and GOME-2) and the Scanning Imaging Absorption spectrometer for Atmospheric Cartography (SCIAMACHY). NASA's Total Ozone Mapping Spectrometer (TOMS), which preceded these instruments, measures the backscattered UV radiation at six wavelengths.

[4] The OMI measurements are used as input to inversion algorithms to retrieve ozone column amount and its vertical distribution, aerosols, clouds, and total column amounts of the trace gases NO_2, SO_2, HCHO, BrO, and OClO.

[5] OMI's prime advantage for aerosol characterization from space is the availability of measurements in the near-UV that can be used for the retrieval of aerosol properties making use of inversion techniques developed for the TOMS sensor. The nearUV technique of aerosol sensing works equally well over all land and water surfaces because of the low UV surface albedo of all ice-snow-free terrestrial surfaces. The availability of UV and visible measurements allows a better characterization of the atmospheric aerosol load. Two aerosol inversion schemes are applied to the OMI measurements; the OMI near-UV (OMAERUV) algorithm uses two UV wavelengths to derive aerosol extinction and absorption optical depth. A multiwavelength algorithm (OMAERO) that uses up to 19 channels in the 330–500 nm spectral range is used to derive aerosol extinction optical depth at several wavelengths.

[6] The OMI measurements are also used to estimate the amount of UV radiation reaching the Earth's surface. The OMI surface UV irradiance algorithm (OMUVB) produces erythemally weighted daily dose, as well as erythemal dose rate and spectral UV irradiances calculated for local solar noon conditions. The erythemal dose rate is calculated by weighting the spectral UV irradiance with the erythemal weighting function [*International Organization for Standardization/Commission Internationale de l'Eclairage*, 1999]. The erythemal daily dose is obtained by integrating the dose rate accumulated over the day. The spectral irradiances are provided at four wavelengths (305.1,

[1] Joint Center for Earth Systems Technology, University of Maryland Baltimore County, Baltimore, Maryland, USA.
[2] Finnish Meteorological Institute, Helsinki, Finland.
[3] Netherlands Royal Meteorological Institute, De Bilt, Netherlands.
[4] Science Systems and Applications, Inc., Lanham, Maryland, USA.
[5] NASA Goddard Space Flight Center, Greenbelt, Maryland, USA.

0148-0227/07/2007JD008809$09.00

Table 1. Number-Weighed Particle Size Distribution Parameters and Real Refractive Index for the Aerosol Types Assumed in the OMI Near-UV Algorithm[a]

Aerosol Model	r_g m1	r_g m2	σ m1	σ m2	Fctn m2	Real	Imaginary
SLF 1–7	0.088	0.509	1.499	2.160	4.04e-4	1.40	.0, 2e-3, 4e-3,6e-3, 8e-3, 1e-2, 1.2e-2
BIO 1–3	0.087	0.567	1.537	2.203	2.06e-4	1.50	0.000, 0.005, 0.010
BIO 4–7	0.080	0.705	1.492	2.075	2.05e-4	1.50	0.020, 0.030, 0.040, 0.048
DST1-7	0.052	0.670	1.697	1.806	4.35e-3	1.55	354 nm: 0, 1.3e-3, 2.6e-3, 5.6e-3, 8.3e-3, 1.3e-2, 2.3e-2 388 nm: 0, 0.9e-4, 1.8e-3, 4.0e-3, 6.0e-3, 9.2e-3, 1.7e-2

[a]Number-weighed particle size distribution parameters: fine and coarse mode radii and variance, coarse mode fraction. The last column shows nodal points in imaginary refractive index (wavelength independent for the sulfate and carbonaceous aerosols and spectrally dependent for desert dust aerosols).

310.1, 324.1, 380.1 nm) assuming triangular slit function with full width half maximum of 0.55 nm. Estimation is based on use of a radiative transfer model whose input parameters are derived from the OMI measurements.

[7] In this paper we present an overview of the aerosol and surface UV products derived from the OMI sensor. The algorithms are briefly described in section 2, followed by a discussion about the current and expected application of these products in section 3. Validation needs and data sets available for validation-evaluation analyses are discussed in section 4, and a summary of validation results presented in other papers of this special section is presented in section 5.

2. Algorithms Overview

2.1. NearUV Aerosol Algorithm

[8] The OMAERUV aerosol algorithm uses measurements made at two wavelengths in the UV region (354 and 388 nm) to take advantage of the large sensitivity of the upwelling radiances to aerosol absorption in this spectral region [*Herman et al.*, 1997; *Torres et al.*, 1998]. The OMAERUV aerosol products are UV Aerosol Index, and aerosol extinction and absorption optical depths at 388 nm.

[9] There are two major advantages of the near-UV technique for deriving aerosols. The reflectance of all terrestrial surfaces (not covered with snow) is small in UV; therefore the retrieval of aerosol properties is possible over a larger variety of land surfaces than in the visible, including the arid and semi-arid regions of the world that appear very bright in the visible and near-IR. The second advantage is the strong interaction between aerosol absorption and molecular scattering from below the aerosol layer that allows one to estimate the aerosol absorption capacity of the atmospheric aerosols [*Torres et al.*, 2005].

[10] In the OMAERUV algorithm the first step is the calculation of the Lambert Equivalent Reflectivity (LER) R^*_{388}, at 388 nm by assuming that the atmosphere scattering is purely Rayleigh, and the atmosphere is bounded by an opaque Lambertian reflector of reflectance R^*_{388}. R^*_{388} is usually larger than the true surface reflectivity (R_{388}) due to scattering from clouds and aerosols but it can be smaller if the aerosols are highly absorbing. The LER at 354 nm is estimated by correcting R^*_{388} for the spectral dependence of surface reflectivity using a pre-computed climatology database (O. Torres et al., Near UV spectral albedo of land and ocean surfaces from TOMS observations, manuscript in preparation, 2007) yielding R^*_{354}.

[11] A key step of the OMAERUV algorithm is the calculation of the UV Aerosol Index (UVAI) as

$$UVAI = -100\ \log_{10}\left[\frac{I^{obs}_{354}}{I^{calc}_{354}\left(R^*_{354}\right)}\right] \quad (1)$$

where I^{calc}_{354} is calculated assuming an LER of R^*_{354}.

[12] The UVAI represents error (expressed in percent divided by 2.3) in estimating satellite radiance at 354 nm from radiance at 388 nm assuming purely molecular atmosphere bounded by a spectrally varying Lambertian surface. The UVAI concept was developed empirically from TOMS observations. Near-zero values of UVAI result when the atmosphere is free of aerosols or when there are large non-absorbing aerosol particles of and clouds present with nearly zero Angstrom coefficient. Aerosols that absorb in the UV (carbonaceous aerosols, desert dust, volcanic ash) are the most important source of positive UVAI values. (Uncorrected spectral variations in surface reflectance, particularly due to sea-glint are another important source). Non-absorbing small particle aerosols yield small negative UVAI values due to their non-zero Angstrom coefficients, but this signal is often buried in noise. Aerosol extinction optical depth (AOD) and aerosol absorption optical depth (AAOD) at 388 nm are derived using a standard inversion algorithm that uses pre-computed reflectances for a set of assumed aerosol models. Three major aerosol types are considered: desert dust (DST), carbonaceous aerosols associated with biomass burning (BIO), and weakly absorbing sulfate-based aerosols (SLF). Each aerosol type is represented by seven aerosol models of varying single scattering albedo, for a total of twenty-one microphysical models. Forward radiative transfer calculations are carried out for each model for a number of nodal points on aerosol layer height and extinction optical depth. The particle size distributions of the twenty-one aerosol models used by OMAERUV are based on observations. The long-term statistics of ground-based measurements by the Aerosol Robotic Network (AERONET) were used to determine the particle size distribution functions required for the forward calculations. Table 1 lists the parameters of the aerosol models used in the inversion.

[13] For a chosen aerosol type, represented by a subset of seven aerosol models, the extinction optical depth and single scattering albedo are retrieved by examining the variability of the relationship between the 354-to-388 nm spectral contrast and the 388 nm reflectance [*Torres et al.*, 1998, 2002a].

[14] The selection of an aerosol type makes use of a combination of spectral and geographic considerations. Since UVAI is largely sensitive only to the UV-absorbing aerosols, it is used to differentiate between carbonaceous and desert dust aerosols, which absorb in the UV, from weakly or non-absorbing aerosols types, such as sulfates, nitrates, and sea-salt. To differentiate between carbonaceous and desert dust aerosols, the algorithm takes advantage of the scene darkening effect of desert dust aerosols in the near UV as explained below.

[15] At 388 nm the scattering and absorption effects of desert dust aerosols nearly cancel so the LER is close to the true surface reflectivity. This absorption is caused by hematite or other iron oxides that are the major UV-absorbing components of desert dust. Carbonaceous aerosols, on the other hand generally increase the LER compared to the true surface reflectivity. Threshold values of the aerosol-related change in LER (R^*_{388}-R_{388}) and the UVAI are used in conjunction with scene type considerations to select an aerosol type.

[16] Since the retrieval algorithm is sensitive to the aerosol height [*Torres et al.*, 1998], results are reported for five different assumptions on the location of the aerosol center of mass: at the surface, and at 1.5, 3.0, 6.0 and 10.0 km above the surface. In addition, best estimate values of AOD and AAOD associated with a particular choice of aerosol vertical distribution are made available. The choice of vertical distribution varies with aerosol type and location. For sulfate-based aerosols the assumed vertical distribution is largest at the surface and decreases exponentially with height. Carbonaceous aerosols layers within 30° of the Equator are assumed to have maximum concentration at 3 km above ground level, whereas mid and high-latitude smoke layers are assumed to peak at 6 km. This step change may produce a discontinuity in the OMI retrieved parameters associated with the possible meridional flow of carbonaceous aerosols across the 30° parallel.

[17] The location of desert dust aerosol layers varies between 1.5 and 10 km, and is given by a multiyear climatological average of Chemical Model Transport (CTM) calculations using the GOCART model [*Ginoux et al.*, 2001] at a lat-lon resolution of $2° \times 2.5°$.

[18] Results are also reported at 354 and 500 nm. The conversions from 388 to 354 and 500 nm are carried out to facilitate comparisons with measurements from other spaceborne and ground-based sensors, as well as with model calculations, which often report values at 500 nm. However, this transformation increases the dependence of the algorithm on the assumed model of aerosols, so the reported values at the other wavelengths, particularly those at 500 nm, should be considered less reliable.

[19] Given the relatively large size of the OMI pixels (compared to sensors specifically designed for aerosol retrieval, such as MODIS), OMI pixels are often cloud contaminated. The effect of subpixel cloud contamination is the overestimation of the extinction optical depth and underestimation of the single scattering co-albedo [*Torres et al.*, 1998]. However, in the calculation of the absorption optical depth a cancellation of errors takes place that allows the AAOD retrieval even in the presence of small amounts of cloud contamination. Thus subpixel cloud contamination is most serious for AOD retrieval. The AAOD is more tolerant of small amounts of cloud contamination and it is therefore the more reliable OMI aerosol product. UVAI is even less affected by clouds, except that it does not provide quantitative estimate of aerosol absorption.

[20] Cloud interference is less of a problem over arid and semi-arid regions where dust aerosols are commonly present. In the presence of cirrus clouds, however, retrievals errors are likely to take place. The effect of optically thin cirrus is similar to that of subpixel cloud contamination discussed above. Cloudless skies are also frequent in areas of seasonal biomass burning and forest fires in the vicinity of the sources. As the plumes of dust and smoke aerosols drift away from their source regions, they get mixed with clouds. This problem is particularly serious over the oceans which are frequently covered with thin cirrus and fair-weather cumulus clouds. Therefore the retrieval of AOD from OMI should be considered reliable only near the source regions.

2.2. Multiwavelength Aerosol Algorithm

[21] The OMI multiwavelength algorithm OMAERO [*Torres et al.*, 2002b] is used to derive aerosol characteristics from OMI spectral reflectance measurements of cloud free scenes at up to 19 wavelengths in the spectral range between 330 nm and 500 nm: 331.7, 340.0, 342.5, 354.0, 367.0, 376.5, 388.0, 399.5, 406.0, 416.0, 425.5, 436.5, 442.0, 451.5, 463.0, 477.0, 483.5, 494.5, and 500.0 nm. These 19 wavelength bands are about 1 nm wide and were chosen such that they are essentially free from strong Raman scattering and gas absorption features except for the band at 477 nm, which comprises an O_2-O_2 absorption band.

[22] Under cloud-free conditions OMI reflectance measurements are sensitive to the aerosol optical depth, the single-scattering albedo, the size distribution, height of the absorbing aerosol layer, and the surface albedo. The sensitivity to the layer height and single scattering albedo is related to the relatively strong contribution of Rayleigh scattering to the measured reflectance in the UV [*Torres et al.*, 1998]. The absorption band of the O_2-O_2 collision complex at 477 nm is used in OMAERO to enhance the sensitivity to the aerosol layer height (B. Veihelmann and J. P. Veefkind, Comparing OMI height data with spaceborne lidar data, manuscript in preparation, 2007) in a way similar to its use in the retrieval of cloud height [*Acarreta et al.*, 2004]. The OMAERO Level 2 data product contains aerosol characteristics such as AOD, aerosol type, aerosol absorption indices as well as ancillary information. The AOD is retrieved from OMI spectral reflectance measurements and a best fitting aerosol type is determined. The single-scattering albedo, the layer height and the size distribution associated with the best fitting aerosol type are provided.

[23] The multiwavelength algorithm uses forward calculations for a number of microphysical aerosol models that are defined by the size distribution and the complex refractive index (see Table 2) as well as the AOD and the aerosol layer height. The models are representative for the main aerosol types desert dust, biomass burning, volcanic and weakly absorbing aerosol. Several subtypes or models represent each of these main types, as listed in Table 2. Synthetic reflectance data have been pre-computed for each aerosol model using the DAK program (Doubling-Adding

Table 2. Size Distributions and Refractive Indices of Aerosol Models Assumed in the OMI Multiwavelength Algorithm[a]

Model	r_g m1	r_g m2	σ m1	σ m2	Fraction	Real	Imaginary
WA_1101	0.078	0.497	1.499	2.160	4.36e-4	1.4	5.0e-8
WA_1102	0.088	0.509	1.499	2.160	4.04e-4	1.4	5.0e-8
WA_1103	0.137	0.567	1.499	2.160	8.10e-4	1.4	5.0e-8
WA_1104	0.030	0.240	2.030	2.030	1.53e-2	1.4	5.0e-8
WA_1201	0.078	0.497	1.499	2.160	4.36e-4	1.4	0.004
WA_1202	0.088	0.509	1.499	2.160	4.04e-4	1.4	0.004
WA_1203	0.137	0.567	1.499	2.160	8.10e-4	1.4	0.004
WA_1301	0.078	0.497	1.499	2.160	4.36e-4	1.4	0.012
WA_1302	0.088	0.509	1.499	2.160	4.04e-4	1.4	0.012
WA_1303	0.137	0.567	1.499	2.160	8.10e-4	1.4	0.012
BB_2101	0.074	0.511	1.537	2.203	1.70e-4	1.5	0.010
BB_2102	0.087	0.567	1.537	2.203	2.06e-4	1.5	0.010
BB_2103	0.124	0.719	1.537	2.203	2.94e-4	1.5	0.010
BB_2201	0.074	0.511	1.537	2.203	1.70e-4	1.5	0.020
BB_2202	0.087	0.567	1.537	2.203	2.06e-4	1.5	0.020
BB_2203	0.124	0. 719	1. 537	2. 203	2.94e-4	1.5	0.020
BB_2301	0.074	0.511	1.537	2.203	1.70e-4	1.5	0.030
BB_2302	0.087	0.567	1.537	2.203	2.06e-4	1.5	0.030
BB_2303	0.124	0.719	1.537	2.203	2.94e-4	1.5	0.030
DD_3101	0.042	0.670	1.697	1.806	4.35e-3	1.53	λ-dep.*
DD_3102	0.052	0.670	1.697	1.806	4.35e-3	1.53	λ-dep.*
DD_3201	0.042	0.670	1.697	1.806	4.35e-3	1.53	λ-dep.#
DD_3202	0.052	0.670	1.697	1.806	4.35e-3	1.53	λ-dep.#
VO_4101	0.230	0.230	0.800	0.800	0.5	1.45	7.5e-7

[a]The main aerosol types, weakly absorbing aerosol (WA), biomass burning aerosol (BB), desert dust (DD), and volcanic (VO) aerosol are divided into subtypes according to size distribution, refractive index, and vertical distribution. Mean radii r_g and variances σ of lognormal number distributions are listed for the modes m1 and m2 of bimodal size distributions together with the particle number fraction of the second mode. The imaginary part of the refractive index of desert dust is wavelength-dependent and takes values up to 6.53e-3 (*) or 0.013 (#) in the UV.

KNMI) [*De Haan et al.*, 1987; *Stammes et al.*, 1989; *Stammes*, 2001] assuming a plane-parallel atmosphere and taking into account multiple scattering as well as polarization. The surface albedo spectrum of land scenes is taken from a global climatology that has been constructed using MISR (Multiangle Imaging Spectroradiometer) data measured in 4 bands (at 446, 558, 672, and 866 nm) that are extrapolated to the UV. The spectral bidirectional reflectance distribution function of ocean surfaces is computed using a model that accounts for the chlorophyll concentration of the ocean water and the near-surface wind speed [*Veefkind and de Leeuw*, 1998].

[24] A principal component analysis applied to synthetic reflectance data was carried out to characterize the capabilities of the multiwavelength algorithm [*Veihelmann et al.*, 2007]. This analysis shows that OMI measurements contain 2 to 4 degrees of freedom of signal. Hence OMI spectral reflectance measurements do not contain sufficient information to retrieve all aerosol parameter independently. In order to constrain the retrieval, a pre-selection of the aerosol models is made before retrieving the AOD for a given scene. For a given ground-pixel this pre-selection can reduce the aerosol models considered in the retrieval to one single aerosol model. In this case the AOD is the only free parameter. In the current implementation major aerosol types are pre-selected on the basis of a climatology of aerosol geographical distribution.The multiwavelength algorithm evaluates the OMI reflectance spectrum viz.

$$\rho(\lambda_l) = \frac{\pi E(\lambda_l)}{\cos(\theta_s) F(\lambda_l)} \tag{2}$$

in a set of wavelength bands, where $E(\lambda_l)$ and $F(\lambda_l)$ are the Earth radiance and the solar irradiance spectrum in the band with a center wavelength λ_l; The index l indicates the wavelength band number; θ_s is the solar zenith angle. In principle, the algorithm could use all the 19 wavelength bands. In the current implementation, however, 14 wavelength bands are chosen. The retrieved aerosol spectral optical depth is reported at the selected wavelengths.

[25] Aerosol parameters are determined by minimizing the merit function Ψ_m

$$\Psi_m = \sum_{l=1}^{L} \left(\frac{\rho^*(\lambda_l) - \rho_m\left(\tau(\lambda_{ref}), \lambda_l\right)}{\varepsilon(\lambda_l)} \right)^2 \tag{3}$$

where $\rho^*(\lambda_l)$ is the measured reflectance, $\rho_m(\tau(\lambda_{ref}), \lambda_l)$ is the reflectance for the aerosol model m as a function of the aerosol optical thickness τ at the reference wavelength λ_{ref}, and $\varepsilon(\lambda_l)$ is the error in the measured reflectance. The merit function is a sum over L wavelength bands. An optimal *AOD* is determined for each model by a non-linear fitting routine using a modified Levenberg-Marquardt method [*More*, 1978]. The best fitting aerosol model with the smallest Ψ_m is selected for the present ground pixel. The retrieved AOD value and precision of the best fitting aerosol model are provided in the OMAERO product. Also, the values of single-scattering albedo, size distribution and aerosol height that are associated with the best fitting aerosol model are provided. Additionally, the aerosol models for which the root mean square of the residual reflectance is below a given threshold are provided together

with the related AOD and assumed single-scattering albedo values.

[26] Cloudy scenes are excluded from the retrieval using three tests. The first test is based on radiance data in combination with the UV aerosol index as defined in section 2.1. The second test uses cloud fraction data from the OMI O_2-O_2 cloud product [*Acarreta and de Haan*, 2002; *Acarreta et al.*, 2004; *Sneep et al.*, 2007]. The third test is based on the spatial homogeneity of the scene.

2.3. Surface UV Algorithm

[27] The OMI surface UV algorithm (OMUVB) is an extension of the TOMS UV algorithm developed at NASA Goddard Space Flight Center (GSFC) [*Eck et al.*, 1995; *Krotkov et al.*, 1998, 2001; *Herman et al.*, 1999; *Tanskanen et al.*, 2006]. The OMUVB algorithm is applied to offline production of the global surface UV data using the OMI TOMS total column ozone [*Bhartia and Wellemeyer*, 2002]. The algorithm is also used in the Very Fast Delivery processing system [*Leppelmeier et al.*, 2006]; there the total column ozone input is retrieved with the OMI DOAS total column ozone algorithm [*Veefkind et al.*, 2006]. The primary contents of the OMUVB product are erythemally weighted daily dose, and erythemal dose rate at local solar noon. Additionally, the product includes spectral irradiances at 305.1, 310.1, 324.1, and 380.1 nm calculated for local solar noon conditions. The spectral irradiances assume triangular slit function with full width half maximum of 0.55 nm. The OMUVB granule contains also additional information, e.g., latitude, longitude, solar zenith angle, and a large number of ancillary parameters relevant for the quality of the data.

[28] Surface UV depends on solar zenith angle, atmospheric ozone, clouds, surface albedo, aerosols and trace gas (e.g., NO_2, SO_2) concentrations, and altitude. The OMI measurements are used as an input for a radiative transfer model to estimate the amount of solar UV radiation reaching the Earth's surface. The OMI surface UV algorithm starts by estimating the surface irradiance assuming clear-sky conditions using basic geophysical information, total column ozone derived from OMI measurements, and climatological surface albedo [*Tanskanen*, 2004]. The obtained clear-sky irradiance is multiplied with a cloud modification factor that accounts for the attenuation of UV radiation by clouds and non-absorbing aerosols. The cloud modification factor is determined by inverting the measured top-of-the-atmosphere radiance into the effective cloud optical depth using a radiative transfer model that assumes a plane-parallel cloud model. The obtained cloud optical depth is used to determine the spectral attenuation effect on surface UV irradiance relative to the clear sky conditions. The current algorithm does not account for absorbing aerosols (e.g., organic carbon, smoke, and dust) or trace gases, which are known to lead to systematic over-estimation of the surface UV irradiance [*Krotkov et al.*, 1998; *Arola et al.*, 2005; *Chubarova*, 2004]. There are plans to implement a correction for absorbing aerosols in the future version of the OMI surface UV algorithm, and the potential of the OMI aerosol products to provide the information required for aerosol correction is being investigated.

[29] The OMI measurements are nominally made once a day around 1:45 p.m. local solar time. However, the spectral and erythemal surface UV irradiances are calculated for solar noon, so that they are comparable to each other, which enable plotting of distribution maps. No correction is made for the change in cloudiness or total column ozone between the local noon and satellite overpass time. The chosen approach has made comparison of the OMI-derived irradiances with ground-based measurements difficult. Therefore there are plans to produce for validation purposes an additional set of OMUVB overpass data, that provide irradiances for the actual OMI observation time. The erythemal daily dose is determined by applying the trapezoidal integration method to the hourly erythemal dose rates calculated assuming the total column ozone and cloud optical depth corresponding to a single OMI measurement. The diurnal cloud variation is major source of uncertainty for daily surface UV doses derived from OMI [*Bugliaro et al.*, 2006]. The OMI surface UV data represent the mean surface UV over a wider region (13 km $\times$ 24 km in nadir) rather than at a point, and therefore the satellite-derived data are not fully comparable with the ground-based measurement data representing local conditions.

3. Data Applications

3.1. Aerosol-Cloud Interaction

[30] A unique UVAI property is the capability of detecting aerosol absorption regardless of the overall scene brightness. The UVAI clearly identifies absorbing aerosols even when intermingled with or above clouds. No other passive remote sensing technique can detect aerosol-cloud mixtures. The UVAI also detects absorbing aerosols above highly reflective scenes such as ice or snow covered surfaces.

[31] This UVAI capability is a valuable tool for studies of the radiative transfer aspects of cloud-aerosol interaction. Studies of the radiative forcing effect of aerosols above clouds [*Liao and Seinfeld*, 1998; *Keil and Haywood*, 2003] indicate that the net direct radiative forcing effect of an absorbing aerosol layer may change from cooling, for cloud-free conditions, to warming when the aerosol layer lies above low-level stratiform clouds. The presence of absorbing aerosol layers above cloud decks is a common occurrence downwind of biomass burning and pollution aerosol sources as in the example shown in Figure 1. The Aqua-MODIS true color image on 13 August 2006 (Figure 1a) shows the presence of an optically dense cloud covering a large region (about 1.4 million square km) in the tropical Atlantic off the coasts of Namibia and Angola. The OMI Aerosol Index in Figure 1b shows the spatial extent of a layer of carbonaceous aerosols flowing westward from the source areas in central Africa above the cloud deck over the ocean. The aerosol absorption optical depth over mostly clear areas as derived from OMI observations is shown in Figure 1c. Values in excess of 0.2 are observed toward the northeast corner of the area in the Figure 1c. The CALIPSO [*Vaughan et al.*, 2004] image in Figure 1d clearly shows the vertical distribution of clouds and aerosols for this particular event. The top of the stratiform cloud layer lies at about 2.0 km above sea level. The aerosol layer above the cloud is confined to a layer between about 2.0 and 5 km above sea level. The total south-north extent of the aerosol deck is about 2600 km, with about half this length lying above a continuous cloud deck.

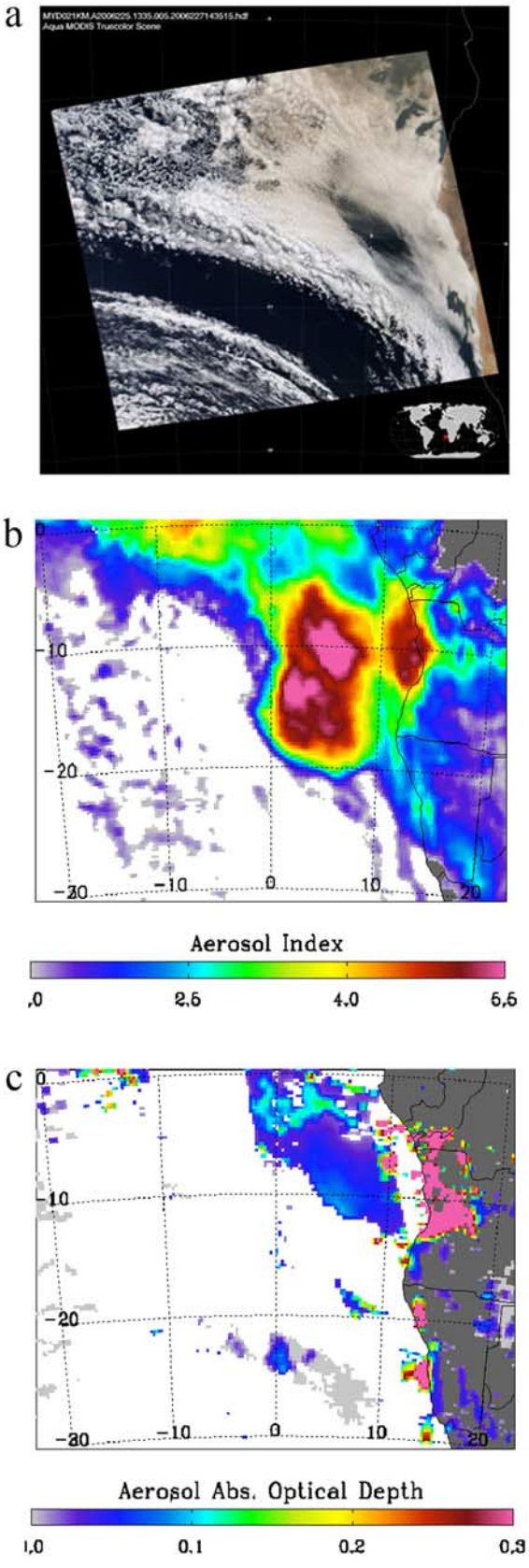

3.2. UTLS Aerosols

[32] The UVAI has been instrumental in the discovery of important aspects of aerosol transport both horizontally and vertically. For instance, UVAI observations indicate that smoke aerosol plumes generated by boreal forest fires at mid and high latitudes are associated with the formation of pyro-cumulonimbus clouds capable of transporting carbonaceous aerosols to the upper troposphere and lower stratosphere (UTLS) regions. Although these aerosols intrusions had been detected by SAGE and POAM observations, their connection to boreal forest fires was unequivocally established by UVAI observations [*Fromm et al.*, 2005]. The value of the UVAI for the identification of these episodes lies on its large sensitivity to the height of the absorbing aerosol layer. An aerosol layer at 10 km and higher yields unusually high values of the UVAI that are always associated with this type of events. One such event took place recently in the Southern Hemisphere when brush fires in Australia triggered the rapid ascent of a convective plume that reached the upper troposphere. This event, clearly observed by several space-based sensors, generated a high-altitude smoke layer that traveled around the world in about 10 days between 14 and 25 December 2006. Figure 2 shows a composite of the OMI AI between 14 and 25 December, as the smoke layer travels westward in a latitudinal zone between 20° and 70°. On 16 and 17 December, the aerosol layer drifts south and reaches Antarctica, where it is clearly observed by the UVAI against the bright Antarctica background. CALIPSO observations indicate that the aerosol layer was confined to a layer between 10 and 14 km. Aerosol Index values as large as 34 were observed at the time of maximum altitude (about 14 km) on December 20 off the coast of Chile.

3.3. Carbonaceous Aerosols Over Europe

[33] The spatial distribution of the synoptic-scale smoke layer generated by the seasonal biomass burning over the Sahel in January 2007 is shown in Figure 3. The horizontal extent of the cloud is depicted in Figure 3a in terms of the Aerosol Index. The unusually large horizontal spread of the smoke layer moving west to the tropical Atlantic Ocean and the Southern Hemisphere, and north as far as Portugal, Spain and France could be associated with changes in atmospheric circulation patterns resulting from El Nino event. Figure 3b shows the cloudiness level, in terms of reflectivity, over the analysis area. Smoke presence is clearly indicated by the AI even when mixed with clouds or above clouds as in the region over Portugal where the AI is significantly larger over the cloud than over the clear

Figure 1. Aerosols over clouds as observed by the MODIS, OMI, and CALIPSO sensors on 16 August 2006 off the west coast of central Africa. Figure 1a shows the Aqua MODIS RGB image indicating the presence of clouds. Figure 1b shows the distribution of aerosols as given by the OMI Aerosol Index. Figure 1c depicts the OMAERUV retrieved aerosol absorption optical depth. Figure 1d shows the vertical profile of attenuated backscatter at 532 nm from CALIPSO observations indicating the presence of absorbing aerosol layer over low-level clouds. See text for details.

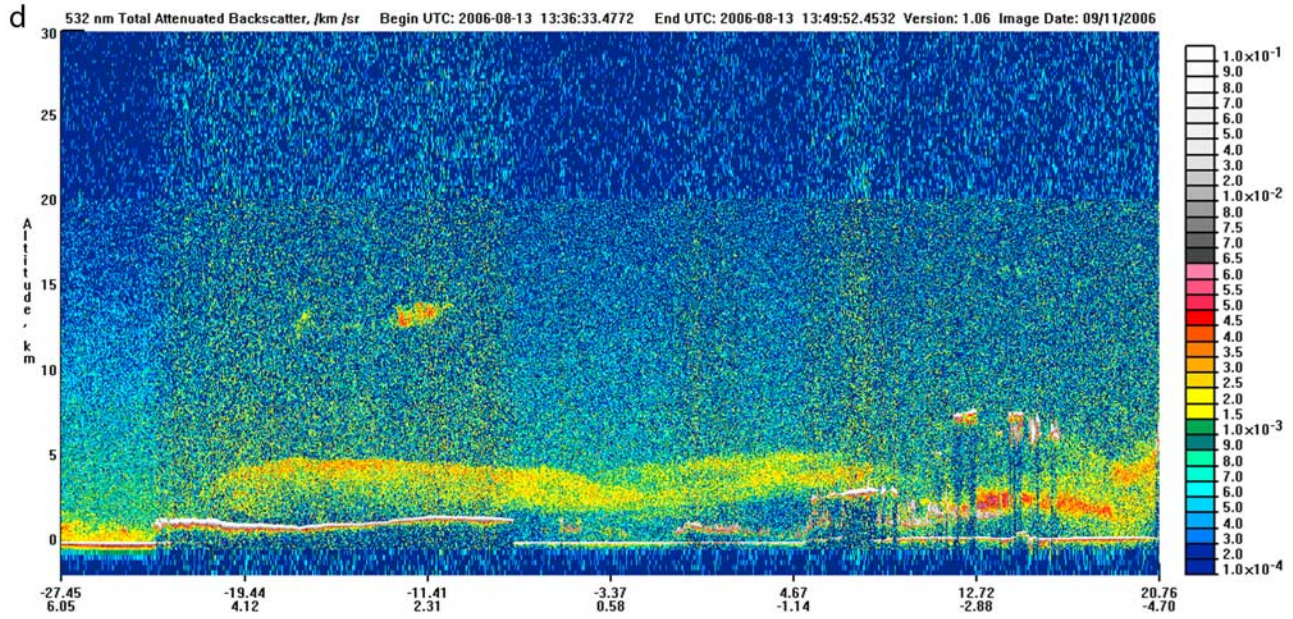

Figure 1. (continued)

areas. The AI enhancement over clouds is an effect resulting from radiative transfers interactions between the bright underlying cloud and the absorbing layer [*Torres et al.*, 1998] and does not represent actual changes in aerosol physical properties.

[34] The retrieval results of extinction and absorption optical depth are shown in Figures 3c and 3d, respectively. The AOD product is affected the most by subpixel cloud contamination resulting in a significant reduction of the spatial coverage as compared to the AI. As discussed in section 2, the AAOD product is more tolerant of small amounts of subpixel cloud contamination, and its spatial coverage is closer to the AI distribution in Figure 3a.

3.4. Global Monitoring of Desert Dust

[35] The seasonal flow of mineral aerosols from the world's major deserts and its trans-oceanic transport across the Atlantic and Pacific Oceans is a well-known phenomenon of importance not just from the climate point of view [*Harrison et al.*, 2001], but also of significance in non-climate related aspects. Dust aerosols may play an important role in heterogeneous atmospheric chemistry processes [*Dentener et al.*, 1996], as well as a modulator of photochemical processes [*Dickerson et al.*, 1997]. The role of trace metals on mineral dust is very important in several marine biogeochemical processes and ocean fertilization. As a source of iron, dust may be a limiting nutrient for phytoplankton [*Fung et al.*, 2000] and therefore play an important role in the modulation of the global carbon cycle. A connection between high desert dust aerosol concentrations and perturbations to the hydrological cycle has been suggested [*Prospero and Lamb*, 2003] on the basis of long-term record of ground-based observations and TOMS Aerosol Index data. OMI Aerosol Index data in 2005 and 2006 has been used in a recent analysis suggesting that changes in sea surface temperature (associated with the shielding effect of the Saharan dust layer) has an influence on the frequency of occurrence of tropical cyclone activity [*Lau and Kim*, 2007].

[36] Daily satellite observations of desert dust at its sources and its transport thousands of kilometers away from their source areas in the African and Asian deserts is one of the most important contributions of the OMI aerosol prod-

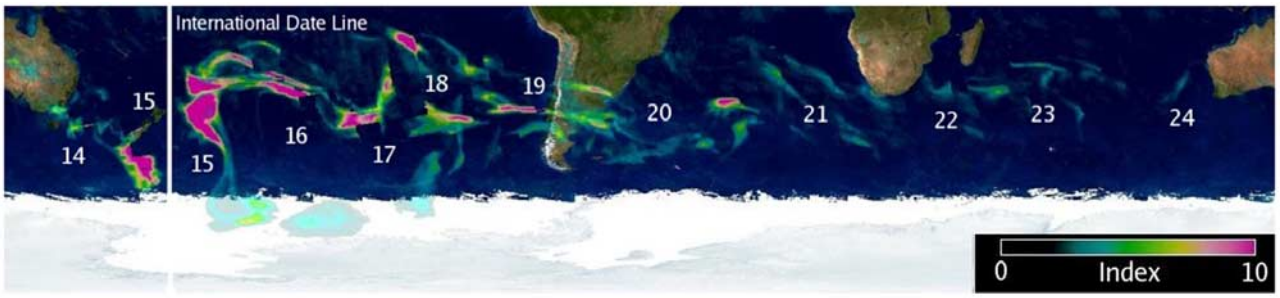

Figure 2. Composite OMI Aerosol Index time series illustrating the transport around the globe of the high-altitude smoke layer generated by the Australian fires in December 2006. Numbers indicate the day of the month.

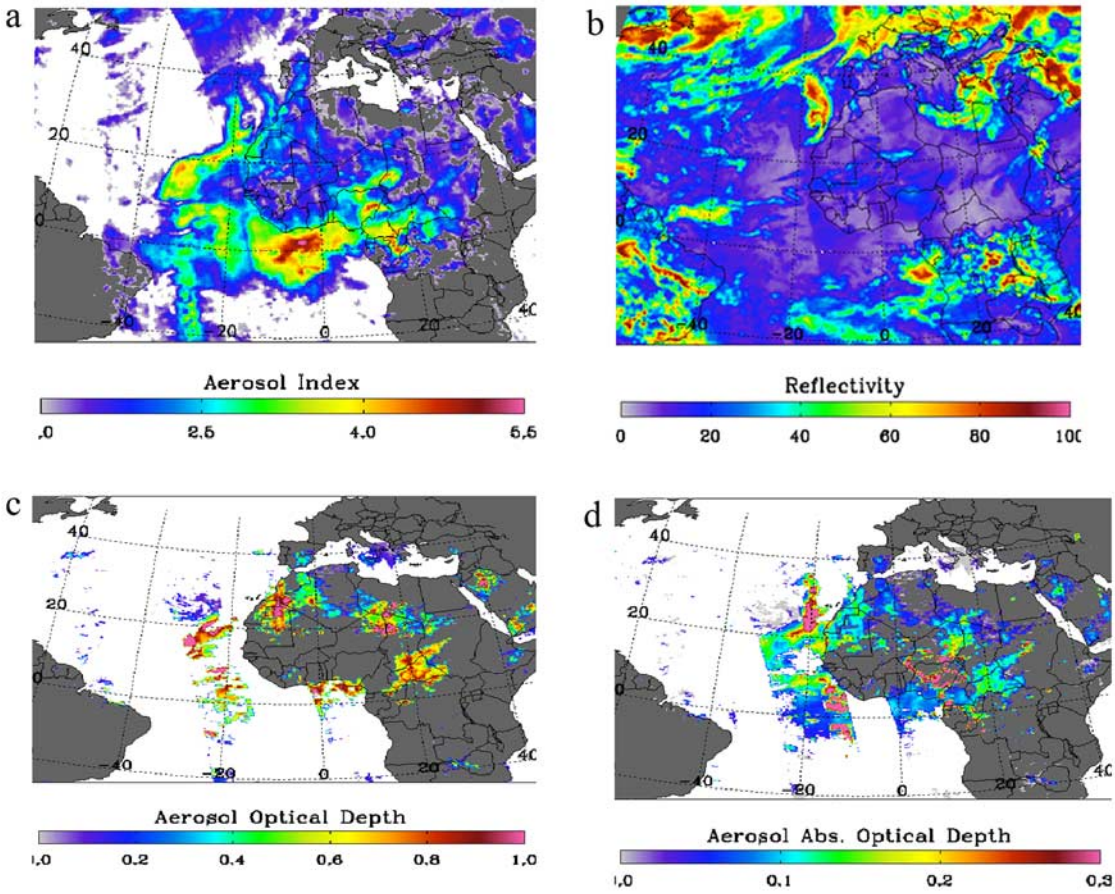

Figure 3. Spatial extent of carbonaceous aerosols on 13 January 2006: (a) Aerosol Index, (b) reflectivity, (c) extinction optical depth, and (d) absorption optical depth.

ucts. Figure 4 shows the Saharan aerosol plume as it flows across the tropical Atlantic Ocean on 15 June 2006. The spatial extent of the plume, even in the presence of clouds is depicted in Figure 4a. The retrieved AAOD (Figure 4b) shows a reduced coverage especially over the oceans due to cloud contamination and sun glint effects. A further reduction in the spatial coverage is observed in the AOD field (Figure 4c). As discussed in section 2, the retrieval error associated with subpixel cloud contamination is largest for the AOD parameter.

3.5. UV Radiation Record

[37] The prime motivation for estimation of surface UV from OMI is to continue the long-term satellite-derived surface UV time series. This global record is used together with ground-based measurement data to assess the long-term changes in surface UV radiation. The satellite-derived surface UV time series extends back to 1978 when the first Nimbus-7/TOMS instrument started to provide UV backscatter measurement data. Thus they cover the decades when the ozone layer, that shields the biosphere from UV radiation, has been endangered by the anthropogenic emissions of ozone depleting compounds.

[38] The global distribution of the clear-sky UV Index on 12 October 2004 derived from the OMI measurements is plotted in Figure 5. It shows elevated surface UV amounts in the southern tip of the South America, which coincides with the breakdown of the southern polar vortex and entering of the ozone depleted polar air masses in to the lower latitudes. Figure 6 shows the erythemal daily surface UV doses in spring 2004 in Ushuaia (54.8S, 68.3W) derived from the OMI measurements and calculated from the ground-based UV measurements of the SUV-100 spectroradiometer of the UV radiation network of the US National Science Foundation. According to the OMI measurements the total column ozone over Ushuaia dropped from 330 Dobson units (DU) on 8 October down to 186 DU on 12 October. This drastic change is also seen in the UV exposure: both the satellite-retrieved and the ground-based surface UV data imply around the 12 October 2004 doses that clearly exceed the climatological UV exposures before the 1980s.

4. Data Sets for Validation and Evaluation of OMI Aerosols and Surface UV

[39] Satellite measurements provide an estimate of the total atmosphere aerosol load in terms of aerosol optical depth. Typically, a direct evaluation of the retrieval product is carried out by a direct comparison of the retrieved parameter to independent temporal and spatial collocated direct measurements of the same quantity. The aerosol contribution to the upwelling radiance at the TOA, however, depends on a number of aerosol microphysical and optical properties (particle size distribution, complex refractive

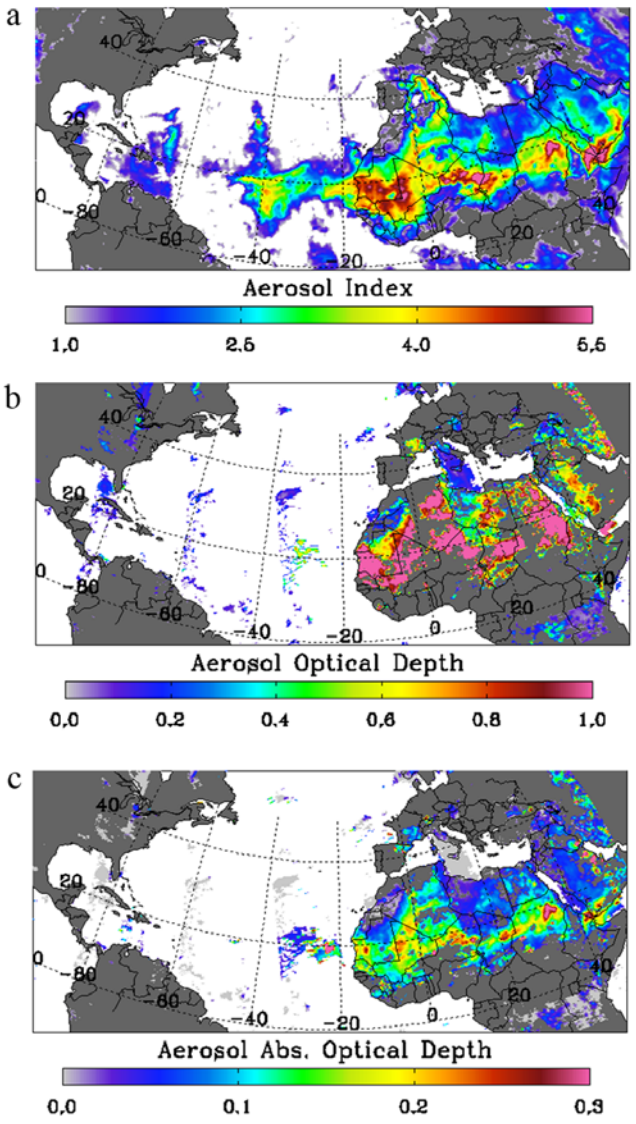

Figure 4. Saharan dust outbreak on 15 June 2006: (a) Aerosol Index, (b) extinction optical depth, and (c) absorption optical depth.

index) as well as environmental conditions (aerosol vertical distribution, surface albedo) and other retrieval-limiting conditions such as signal contamination from non-aerosol factors (subpixel clouds and ocean color). Since it is not possible to simultaneously derive all this information from the satellite measurements, it is necessary to make assumptions or use external data. Thus, in assessing the quality of the final retrieval product, the validity of those assumptions should also be examined, especially when the assumptions are not firmly based on observational data.

4.1. Aerosol Optical Depth Data Sets

[40] Ground-based measurements of aerosol extinction optical depth are the most widely available data for the validation of satellite measurements of the atmospheric aerosol load. AERONET [*Holben et al.*, 1998] is a worldwide network of CIMEL Sun photometers that measures AOD at a number of wavelengths at 15 minutes intervals. AERONET operates a 4-wavelength instrument (440, 675, 870 and 1020 nm), and a 7-wavelenghth sensor (340, 380, 440, 500, 675, 870 and 1020 nm). Most of the currently operating AERONET sites, however, are equipped with 7-wavelength instrumentation. Although most AERONET measurements are representative of continental aerosol types, a few island and coastal area stations [*Smirnov et al.*, 2003] are considered representative of maritime aerosol conditions than can be used for validation of satellite retrievals over the oceans.

[41] Airborne measurements of aerosol optical depth are another important type of observations available for validation of satellite retrievals. The fourteen-wavelength Ames Airborne Tracking Sun photometer [*Russell et al.*, 2005] measures the vertical distribution of the atmospheric aerosol load (in terms of extinction coefficient) as well as the column amount integrated down to the flight level. The AATS-14 spectral range includes four wavelengths (354, 380, 453, and 499) in the OMI spectral coverage. Since the launch of OMI in mid-2004, the AATS-14 was flown on INTEX-B/MILAGRO campaigns. In addition to providing total optical depth measurements, the AATS-14 also provides important information on the aerosol vertical distribution, an important factor in the retrieval of absorbing aerosol properties using OMI near-UV observations. The airborne optical depth measurements are particularly useful for the validation of satellite retrievals over the oceans where the surface-based measurements are scarce.

4.2. Aerosol Optical Properties Data Sets

[42] AERONET direct sun measurements of spectral optical depth and angular observations of sky radiances at four wavelengths (440, 670, 870 and 1020 nm) are fed to an inversion procedure to retrieve fine and coarse modes of the aerosol particle size distribution, and the complex refractive index of the aerosol column. The aerosol particle size distribution and optical properties are derived by fitting measurements of the spectral AOD and sky radiances to radiative transfer calculations [*Dubovik and King*, 2000]. The retrieved complex refractive index and PSD parameters are used in the calculation of the single scattering albedo and absorption optical depth that can be directly used for comparison to the OMI retrievals. Similar comparison has been carried out for the evaluation of TOMS retrievals of aerosol absorption [*Torres et al.*, 2005]. These retrieved aerosol properties from ground-based remote sensing are very useful for the evaluation of assumptions regarding the aerosol models in the satellite inversion algorithms. The AERONET derived database on single scattering albedo is the only set of observations available for assessing the accuracy of the aerosol absorption information derived by the OMI near UV algorithm.

4.3. Aerosol Vertical Distribution Data Sets

[43] Lidar measurements are the most suitable data for the accurate representation of the aerosol vertical distribution. The Micropulse Lidar Network, MPLNET [*Welton et al.*, 2001] and the European Lidar Network, EARLINET [*Bösenberg et al.*, 2001] are two important sources of ground-based observations of the vertical distribution of aerosol particles. The MPLNET database includes information from 26 sites around the world. Thirteen MPLNET sites

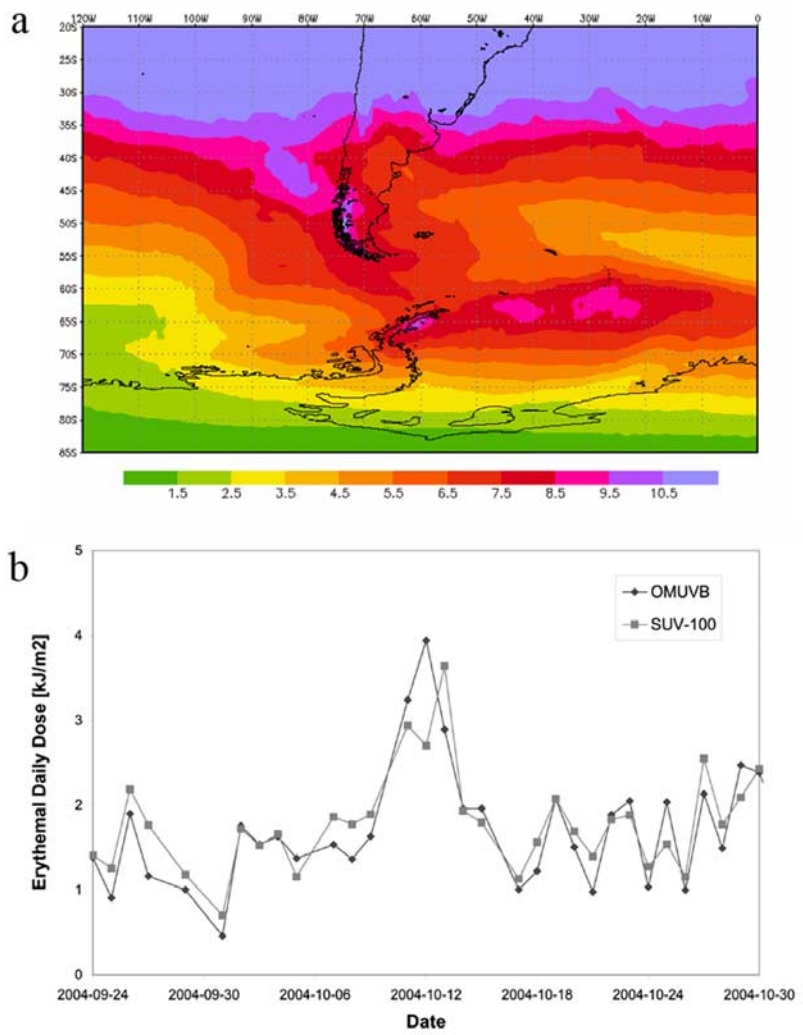

Figure 5. (a) Distribution of the clear-sky UV Index in the southern part of South America and Antarctic Peninsula on 12 October 2004 derived from the OMI measurements. (b) Erythemal daily surface UV doses in spring 2004 in Ushuaia derived from the OMI measurements and calculated from the ground-based UV measurements of the NSF's SUV-100 spectroradiometer.

have operated at least temporarily in the 2005–2006 period providing useful data during the OMI period of operation. The EARLINET lidar database includes 25 stations in Europe, most of which have been operational during the 2005–06 period. Space-based aerosol lidar information is also currently available from CALIPSO (Cloud-Aerosol Lidar and Infrared Pathfinder Satellite Observations) a combination of an active sensor with passive infrared and visible imagers to probe the vertical structure and properties of thin clouds and aerosols over the globe [*Vaughan et al.*, 2004] with day and nighttime lidar observations at 532 and 1064 nm. Polarization measurements at the two channels are also available. CALIPSO revolves around the Earth in fly formation with other sensors in the A-train. The quasi-simultaneity of OMI and CALIPSO measurements (CALIPSO overpass takes place five minutes earlier than Aura's), make the CALIPSO data suitable not only for validation of OMI assumptions on aerosol vertical distribution, but also for actual synergistic use of both measurements in retrieval algorithms. Another currently operating satellite-borne lidar is the Geoscience Laser Altimeter System (GLAS) on the IceSat spacecraft [*Zwally et al.*, 2002], launched in January 2003. Although the frequency of observations have greatly diminished due to the early failure of the 532 nm laser, measurements at 1064 have been made since the launch of OMI. GLAS measurements in the period July 2004 to July 2006 (prior to the deployment of CALIPSO) could be particularly useful in the evaluation of OMI observations.

4.4. A-Train Sensors

[44] In addition to the active remote sensing from CALIPSO measurements, a wealth of additional quasi-simultaneous information for the assessment of OMI aerosol products is available from other passive sensors operating on A-train platforms. PARASOL flying just five minutes ahead of Aura provides optical depth at 670 and 865 nm for fine and coarse mode aerosols over the oceans, and for fine mode aerosols over land. PARASOL also derives a non-sphericity index particularly useful in the identification of mineral aerosols. The Aura spacecraft flies only eight

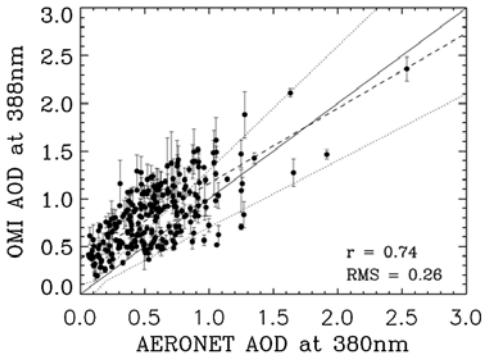

Figure 6. Comparison of AERONET measured to OMAERUV retrieved aerosol optical depth at four AERONET desert dust sites: Blida (36N, 2E), Dakar (14N, 16W), Hamim (22N, 54E), and Saada (31N, 8W). The original AERONET measurements at 441 nm have been converted to 380 nm using AERONET's Angstrom parameter. The one-to-one is represented by the solid line. The dotted lines represent the expected uncertainty (larger of 0.1 or 30%). The dashed line is a linear fit. The correlation coefficient is 0.74, and the root mean square error is 0.26.

minutes behind Aqua. Aqua-MODIS aerosol information consists of aerosol optical depth over the ocean and most land areas, as well as information on particle size. The AIRS sensor, also on Aqua, provides information on the presence of desert dust aerosols that interfere with their temperature retrieval [*DeSouza-Machado et al.*, 2006]. These data sets are important for the evaluation of OMI aerosol products, and also potentially they can be integrated in retrieval approaches that take advantage of the particular strengths of each sensor.

4.5. Surface UV Data Sets

[45] The most important reference data used in validation are the ground-based surface UV measurements. The validation sites should represent various latitudes, climatic conditions, land cover types and altitudes. Since the OMI surface UV algorithm is based on radiative transfer modeling, all the auxiliary information on atmospheric and surface conditions are useful for checking the validity of the assumptions made in modeling. For example some validation sites provide concurrent measurements of aerosol optical depth and single scattering albedo that can be used to validate surface UV algorithm to account for aerosols. Similarly all the information on ozone and its profile as well as on clouds or trace gases can help in identifying the possible causes of the differences.

[46] Various instruments are used for monitoring of the UV radiation reaching the Earth's surface [*World Meteorological Organization*, 2007, section 7.3.1]. Currently spectroradiometers are considered the most accurate and versatile instruments to provide reference data for validation of the satellite-derived surface UV. They typically provide tens of UV spectra per day with wavelength resolution of 0.5–1 nm. Spectral UV measurement data are available from two major databases: the World Ozone and Ultraviolet Radiation Data Centre (WOUDC) for 29 stations, and the European Ultraviolet Database (EUVDB) for 43 stations. Additionally, many networks maintain their own databases: for example the UV measurements of the US National Science Foundation's UV monitoring network data are easily available together with auxiliary data (total column ozone, effective albedo, cloud optical depth) derived from the measured spectra. The auxiliary data are very useful in interpretation of the validation results.

[47] Surface UV irradiance has been derived from many satellite instruments using various methods. For example the solar UV backscatter measurements of the TOMS series, ERS/GOME-1, and ENVISAT/SCIAMACHY instruments have been used to estimate the surface UV irradiances [*Eck et al.*, 1995; *Meerkötter et al.*, 1997; *Lubin et al.*, 1998; *Herman et al.*, 1999; *Verdebout*, 2000; *Van Geffen et al.*, 2004]. In the near future the Metop/GOME-2 measurements will be used for surface UV estimation [*Kujanpää et al.*, 2006]. Sometimes the attenuation of the UV radiation by clouds have been estimated using the same satellite data as was used for obtaining the total column ozone, but often, the AVHRR and MVIRI measurements have been used to estimate the cloud attenuation. The inter-comparisons of the coexistent satellite-derived surface UV data are useful for identification of the possible systematic differences between the algorithms. Furthermore, in order to study the long-term changes in surface UV radiation there is a need to combine multiple satellite-derived surface UV time series, which requires elimination of the systematic differences between the different data sets.

5. Evaluation Results

[48] Several validation and evaluation analysis of the OMI aerosols and surface UV products have been conducted and their results are published in separate papers of this special section. A brief overview of those results is presented in this section.

5.1. Near UV Aerosol Product

[49] The performance of the OMAERUV algorithm was evaluated making use of ground-based AERONET measurements as well as satellite observations by the Aqua-MODIS and Terra-MISR sensors.

[50] AERONET ground-based direct sun measurements of aerosol optical depth as well as values of retrieved single scattering albedo at a large numbers of sites around the world are used in the assessment of the OMAERUV aerosol products (O. Torres et al., Evaluation of OMI UV aerosol products using AERONET observations, submitted to *Journal of Geophysical Research*, 2007; hereinafter referred to as Torres et al., submitted manuscript, 2007). The AOD comparison indicates that the OMAERUV retrieval is severely affected by subpixel cloud contamination. Under conditions of minimum cloud interference reasonable AERONET-OMAERUV comparisons are found. Thus OMAERUV AOD retrievals are more accurate for arid and semi-arid environments during the seasons of active aerosol production when the atmospheric aerosol load is large and the effect of cloud contamination is not significant. The scatterplot in Figure 6 shows the resulting AERONET-OMAERUV AOD comparison at a number of sites in sub-Saharan Africa. For details of the analysis, see Torres et al. (submitted manuscript, 2007). The OMAERUV

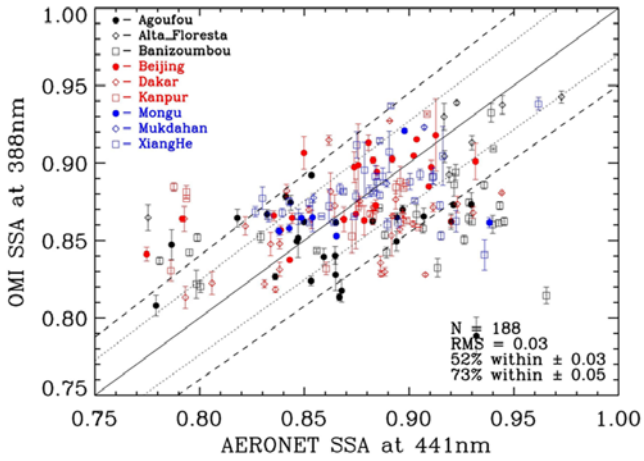

Figure 7. Scatterplot of retrieved single scattering albedo by AERONET (x axis) and OMAERUV algorithm (y axis) at 9 AERONET sites. Solid line represents the one-to-one. The dotted lines indicate the domain where the two retrievals agree with each other within 0.03. The dashed line indicates agreement within 0.05. A total of 188 retrievals are plotted, yielding a root mean square error of 0.03.

aerosol absorption product was also evaluated with the AERONET retrievals of aerosol single scattering albedo. Comparisons of single scattering albedo for carbonaceous aerosols show that the ground-based approach and the satellite technique agree quite well with each other yielding root mean square differences of 0.03. Figure 7 shows the comparison of retrieved single scattering albedo over a variety of AERONET sites in Africa, Asia and South America. Similar comparisons for desert dust aerosols indicate a very close relationship between the two retrievals yielding RMS difference of 0.02.

[51] C. Ahn et al. (Comparison of OMI UV aerosol products with Aqua-MODIS and MISR observations in 2006, submitted to *Journal of Geophysical Research*, 2007; hereinafter referred to as Ahn et al., submitted manuscript, 2007) carried out an evaluation of the OMAERUV product using satellite-derived aerosol optical depth from other sensors. Collocated OMAERUV-MODIS AOD measurements are reasonably well correlated. Regional comparisons of the annual aerosol cycle as derived by Aqua-MODIS, Terra-MISR and OMI show good agreement over most of the area in the analysis.

5.2. Multiwavelength Aerosol Product

[52] R. L. Curier et al. (Retrieval of aerosol optical properties from OMI radiances using a multiwavelength algorithm: Application and validation to western Europe, submitted to *Journal of Geophysical Research*, 2007; hereinafter referred to as Curier et al., submitted manuscript, 2007) have performed a validation study of the OMAERO aerosol optical depth data for the 2005 summer. In this validation study ground-based in situ, AERONET Sun photometer and data from the Aqua-MODIS satellite instrument have been used. Because the spectral surface albedo is one of the major uncertainties in the OMAERO algorithm, the spectral surface albedo is derived for the Cabauw measurement site in the Netherlands for the DANDELIONS field campaign, using a combination of ground-based observations and OMI data. The surface climatology used is in good agreement with the derived spectral surface albedo. A favorable agreement has been found between OMAERO data and AERONET data for the aerosol optical thickness. Evidence is found that for arid regions (e.g., Spain and Portugal) the aerosol optical thickness over land is overestimated, because the surface albedo is underestimated. The aerosol optical thickness from MODIS correlates well with the OMAERO data. This correlation is higher over the ocean than over land. It has been observed that the OMAERO multiwavelength algorithm tends to overestimate the aerosol optical thickness, while trends are rendered well.

[53] Additional OMAERO validation efforts have been undertaken during the second DANDELIONS (Dutch Aerosol and Nitrogen Dioxide Experiments for vaLIdation of OMI and SCIAMACHY) validation campaign, held at the Cabauw Experimental Site for Atmospheric Research in Netherlands in 2006 (E. J. Brinksma et al., NO_2 and aerosol validation during the 2005 and 2006 DANDELIONS campaigns, submitted to *Journal of Geophysical Research*, 2007; hereinafter referred to as Brinksma et al., submitted manuscript, 2007). The correspondence between AOT values measured with the ground-based Sun photometers with those retrieved from OMI measurements are excellent, considering the difference in techniques, although it must be said that the statistics are quite poor. Comparisons between OMI and ground-based instruments will be extended to longer time series, as well as to other ground sites.

5.3. Surface UV Product

[54] *Tanskanen et al.* [2007] compared the OMI-derived daily erythermal doses to the daily doses calculated from the ground-based spectral UV measurements from 18 reference instrument. They found that for flat, snow-free regions with modest loadings of absorbing aerosols or trace gases the OMI-derived daily erythemal doses are 0 to 10% overestimated and some 70% of the doses agree within ±20% with the reference dose. However, for some validation sites the OMI-derived daily doses were found to diverge substantially from the reference data. For sites significantly affected by absorbing aerosols or trace gases one expects bigger positive bias up to 50%. For high-latitude sites the satellite-derived doses are occasionally up to 50% too small because of unrealistically small climatological surface albedo. They conclude that the two key priorities in further development of the OMI surface UV algorithm are to introduce a correction to account for absorbing aerosols and trace gases, and to improve the quality of the assumed surface albedo. There are several further studies in progress that focus on validation of the spectral irradiances with the aim of clarifying the role of aerosols and trace gases on surface UV irradiance.

6. Summary and Conclusions

[55] A general overview of the aerosol and surface UV products from the Aura Ozone Monitoring Instrument has been presented in this paper. For almost three years after launch, the OMI sensor has been successfully extending the

multiyear-long on aerosols and surface UV radiation available from observations by the TOMS sensor since 1978.

[56] As in the TOMS aerosol algorithm the OMI near-UV aerosol inversion procedure takes full advantage of the well-documented sensitivity of UV measurements to aerosol absorption [*Torres et al.*, 1998, 2005]. OMAERUV retrieval products consist of the Aerosol Index, and aerosol extinction and absorption optical depth at 388 nm. OMAERUV seeks to extend the near-UV aerosol absorption record available from TOMS since 1978. An assessment of the performance of OMAERUV has been carried out using ground-based observations of aerosol optical depth and single scattering albedo (Torres et al., submitted manuscript, 2007). Results of this comparison indicate that subpixel cloud contamination is a large source of uncertainty in the derivation of extinction optical depth. As expected, for environments where cloud contamination is not significant, better agreement was found between the ground measurements and OMAERUV retrievals. A particularly encouraging result is the comparison of OMAERUV and AERONET retrieved aerosol single scattering albedo that yields root mean square differences of 0.03. On a larger spatial scale, OMAERUV retrievals of aerosol extinction optical depth have also been evaluated by comparison to MODIS and MISR retrievals (Ahn et al., submitted manuscript, 2007). Reasonable agreement between OMAERUV and the other two sensors was found. The multiwavelength aerosol algorithm (OMAERO) uses a spectral fitting approach that seeks to exploit the UV-to-visible OMI spectral coverage for aerosol characterization. In this spectral range there is sensitivity to aerosol absorption in the near-UV region, and to aerosol layer height in the near UV and in the absorption band of the O_2-O_2 collision complex at 477 nm. These sensitivities allow OMAERO to identify realistic aerosol models that are used in the retrieval of aerosol extinction optical depth at several wavelengths in the range 354–500 nm. OMAERO retrieval results have been evaluated using AERONET ground-based measurements and MODIS retrievals in Western Europe (Curier et al., submitted manuscript, 2007; Brinksma et al., submitted manuscript, 2007). The most important factors affecting the retrieval quality are subpixel cloud contamination and the prescribed spectral surface albedo.

[57] The OMI-derived surface UV product provides continuation to the widely used long-term record of surface UV based on the series of TOMS instruments. Validation analysis reported in this special section [*Tanskanen et al.*, 2007] shows that the OMI-derived surface UV estimates are accurate for flat, snow-free regions with low concentrations of absorbing aerosols or trace gases in the atmosphere. However, the algorithm could be significantly improved by introducing a correction to account for absorbing aerosols and trace gases, and by improving the quality of the surface albedo climatology.

[58] **Acknowledgments.** The Dutch-Finnish–built OMI instrument is part of the NASA EOS Aura satellite payload. The OMI project is managed by NIVR and KNMI in Netherlands. The OMI data are obtained from the Goddard Earth Sciences Distributed Active Archive Center, http://disc.gsfc.nasa.gov. We thank the CALIPSO science team for the imagery used in this paper. We also thank Colin Seftor of SSAI for his assistance with the graphics.

References

Acarreta, J. R., and J. F. de Haan (2002), Cloud pressure algorithm based on O_2-O_2 absorption, in *OMI Algorithm Theoretical Basis Document*, vol. 3, *Clouds, Aerosols and Surface UV Irradiance, ATBD-OMI-03*, edited by P. Stammes and R. Noordhoek, pp. 17–30, NASA, Washington D. C.

Acarreta, J. R., J. F. De Haan, and P. Stammes (2004), Cloud pressure retrieval using the O_2-O_2 absorption band at 477 nm, *J. Geophys. Res.*, *109*, D05204, doi:10.1029/2003JD003915.

Arola, A., S. Kazadzis, N. Krotkov, A. Bais, J. Gröbner, and J. R. Herman (2005), Assessment of TOMS UV bias due to absorbing aerosols, *J. Geophys. Res.*, *110*, D23211, doi:10.1029/2005JD005913.

Bhartia, P. K., and C. W. Wellemeyer (2002), TOMS-V8 total O3 algorithm, in *OMI Algorithm Theoretical Basis Document*, vol. II, edited by P. K. Bhartia, pp. 15–32, NASA Goddard Space Flight Cent., Greenbelt, Md. (Available at http://eospso.gsfc.nasa.gov/eos_homepage/for_scientists/atbd/docs/OMI/ATBD-OMI-02.pdf)

Bösenberg, J., et al. (2001), EARLINET: A European aerosol research lidar network, in *Laser Remote Sensing of the Atmosphere, Selected Papers of the 20th International Laser Radar Conference, Vichy, France*, edited by A. Dabas, C. Loth, and J. Pelon, pp. 155–158, Ecole Polytech., Paris.

Bugliaro, L., B. Mayer, R. Meerkötter, and J. Verdebout (2006), Potential and limitations of space-based methods for the retrieval of surface UV-B daily doses: A numerical study, *J. Geophys. Res.*, *111*, D23207, doi:10.1029/2005JD006534.

Chubarova, N. E. (2004), Influence of aerosol and atmospheric gases on ultraviolet radiation in different optical conditions including smoky mist of 2002, *Dokl. Earth Sci.*, *394*(1), 62–67.

De Haan, J., P. Bosma, and J. Hovenier (1987), The adding method for multiple scattering computations of polarized light, *Astron. Astrophys.*, *183*, 371–391.

Dentener, F. J., G. R. Carmichael, Y. Zhang, J. Lelieveld, and P. J. Crutzen (1996), Role of mineral aerosols as a reactive surface in the global troposphere, *J. Geophys. Res.*, *101*, 22,869–22,889.

DeSouza-Machado, S. G., L. L. Strow, S. E. Hannon, and H. E. Motteler (2006), Infrared dust spectral signatures from AIRS, *Geophys. Res. Lett.*, *33*, L03801, doi:10.1029/2005GL024364.

Dickerson, R. R., S. Kondragunta, G. Stenchikov, K. L. Civerolo, B. G. Doddridge, and B. N. Holben (1997), The impact of aerosols on solar ultraviolet radiation and photochemical smog, *Science*, *278*, 827–830.

Dubovik, O., and M. D. King (2000), A flexible inversion algorithm for retrieval of aerosol optical properties from Sun and sky radiance measurements, *J. Geophys. Res.*, *105*(D16), 20,673–20,696.

Eck, T. F., P. K. Bhartia, and J. B. Kerr (1995), Satellite estimation of spectral UVB irradiance using TOMS derived ozone and reflectivity, *Geophys. Res. Lett.*, *22*, 611–614.

Fromm, M., R. Bevilacqua, R. Servranckx, J. Rosen, J. P. Thayer, J. Herman, and D. Larko (2005), Pyro-cumulonimbus injection of smoke to the stratosphere: Observations and impact of a super blowup in northwestern Canada on 3–4 August 1998, *J. Geophys. Res.*, *110*, D08205, doi:10.1029/2004JD005350.

Fung, I., S. Meyn, I. Tegen, S. C. Doney, J. John, and J. K. B. Bishop (2000), Iron supply and demand in the upper ocean, *Global Biogeochem. Cycles*, *14*, 281–296.

Ginoux, P., M. Chin, I. Tegen, J. Prospero, B. Holben, D. Dubovik, and S. J. Lin (2001), Sources and distributions simulated with the GOCART Model, *J. Geophys. Res.*, *106*, 20,255–20,273.

Harrison, S. P., K. E. Kohfeld, C. Roelandt, and T. Claquin (2001), The role of dust in climate changes today, at the Last Glacial Maximum and in the future, *Earth Sci. Rev.*, *54*, 43–80.

Herman, J. R., P. K. Bhartia, O. Torres, C. Hsu, C. Seftor, and E. Celarier (1997), Global distribution of UV-absorbing aerosols from Nimbus-7/TOMS data, *J. Geophys. Res.*, *102*, 16,911–16,922.

Herman, J. R., N. Krotkov, E. Celarier, D. Larko, and G. Labow (1999), Distribution of UV radiation at the Earth's surface from TOMS-measured UV-backscattered radiances, *J. Geophys. Res.*, *104*(D10), 12,059–12,076.

Holben, B. N., et al. (1998), AERONET—A federated instrument network and data archive for aerosol characterization, *Remote Sens. Environ.*, *66*, 1–16.

International Organization for Standardization/Commission Internationale de l'Eclairage (1999), Erythema reference action spectrum and standard erythema dose, *ISO 17166:1999 (E) CIE S 007/E-1998*, CIE Cent. Bur., Vienna.

Keil, A., and J. M. Haywood (2003), Solar radiative forcing by biomass burning aerosol particles during SAFARI 2000: A case study based on measured aerosol and cloud properties, *J. Geophys. Res.*, *108*(D13), 8467, doi:10.1029/2002JD002315.

Krotkov, N. A., P. K. Bhartia, J. R. Herman, V. Fioletov, and J. Kerr (1998), Satellite estimation of spectral surface UV irradiance in the presence of tropospheric aerosols: 1. Cloud-free case, *J. Geophys. Res.*, *103*, 8779–8793.

Krotkov, N. A., P. K. Bhartia, J. R. Herman, Z. Ahmad, and V. Fioletov (2001), Satellite estimation of spectral surface UV irradiance: 2. Effect of horizontally homogeneous clouds and snow, *J. Geophys. Res.*, *106*, 11,743–11,759.

Kujanpää, J., A. Määttä, J. Kaurola, T. Koskela, K. Lakkala, and A. Karpetchko (2006), Operational surface UV product and validation service of ozone and atmospheric chemistry monitoring SAF, paper presented at 2006 EUMETSAT Meteorological Satellite Conference, Eur. Organ. for the Exploit. of Meteorol. Satel., 12 –16 June , Helsinki.

Lau, W. K. M., and K. M. Kim (2007), How nature foiled the 2006 hurricane forecasts, *Eos Trans. AGU*, *88*(9), 105.

Leppelmeier, G. W., O. Aulamo, S. Hassinen, A. Mälkki, T. Riihisaari, R. Tajakka, J. Tamminen, and A. Tanskanen (2006), OMI Very Fast Delivery and Sodankylä Satellite Data Centre, *IEEE Trans. Geosci. Remote Sens.*, *44*(5), 1283–1287.

Levelt, P. F., E. Hilsenrath, G. W. Leppelmeier, G. H. J. van den Oord, P. K. Bhartia, J. Taminnen, J. F. de Haan, and J. P. Veefkind (2006), Science objectives of the Ozone Monitoring Instrument, *IEEE Trans. Geosci. Remote Sens.*, *44*(5), 1093–1101.

Liao, H., and J. H. Seinfeld (1998), Effect of clouds on direct aerosol radiative forcing of climate, *J. Geophys. Res.*, *103*(D4), 3781–3788.

Lubin, D., E. H. Jensen, and H. P. Gies (1998), Global surface ultraviolet radiation climatology from TOMS and ERBE data, *J. Geophys. Res.*, *103*(D20), 26,061–26,092.

Meerkötter, R., B. Wissinger, and G. Seckmeyer (1997), Monitoring surface UV from ERS-2/GOME and NOAA/AVHRR data: A case study, *Geophys. Res. Lett.*, *25*(15), 1939–1942.

More, J. J. (1978), The Levenberg-Marquardt algorithm: Implementation and theory, in *Numerical Analysis Proceedings (Dundee, June 28–July 1, 1977)*, *Lecture Notes Math.*, vol. 630, edited by G. A. Watson, pp. 105–116, Springer, New York.

Prospero, J. M., and P. J. Lamb (2003), African droughts and dust transport to the Caribbean: Climate change implications, *Science*, *32*, 1024–1026.

Russell, P., et al. (2005), Aerosol optical depth measurements by airborne sun photometer in SOLVE II, *Atmos. Chem. Phys.*, *5*, 1311–1339, SRef-ID:1680-7324/acp/2005-5-1311.

Smirnov, A., B. N. Holben, O. Dubovik, R. Frouin, T. F. Eck, and I. Slutsker (2003), Maritime component in aerosol optical models derived from Aerosol Robotic Network data, *J. Geophys. Res.*, *108*(D1), 4033, doi:10.1029/2002JD002701.

Sneep, M., J. F. de Haan, P. Stammes, P. Wang, C. Vanbauce, J. Joiner, A. P. Vasilkov, and P. F. Levelt (2007), Three-way comparison between OMI and PARASOL cloud pressure products, *J. Geophys. Res.*, doi:10.1029/2007JD008694, in press.

Stammes, P. (2001), Spectral radiance modelling in the UV-visible range, in *IRS 2000: Current Problems in Atmospheric Radiation*, edited by W. L. Smith and Y. M. Timofeyev, pp. 385–388, A. Deepak, Hampton, Va.

Stammes, P., J. de Haan, and J. Hovenier (1989), The polarized internal radiation field of a planetary atmosphere, *Astron. Astrophys.*, *225*, 239–259.

Tanskanen, A. (2004), Lambertian surface albedo climatology at 360 nm from TOMS data using moving time-window technique, paper presented at XX Quadrennial Ozone Symposium, Int. Ozone Comm., 1 –8 June Kos, Greece.

Tanskanen, A., N. A. Krotkov, J. R. Herman, and A. Arola (2006), Surface ultraviolet irradiance from OMI, *IEEE Trans. Geosci. Remote Sens.*, *44*(5), 1267–1271.

Tanskanen, A., et al. (2007), Validation of daily erythemal doses from Ozone Monitoring Instrument with ground-based UV measurement data, *J. Geophys. Res.*, doi:10.1029/2007JD008830, in press.

Torres, O., P. K. Bhartia, J. R. Herman, and Z. Ahmad (1998), Derivation of aerosol properties from satellite measurements of backscattered ultraviolet radiation: Theoretical basis, *J. Geophys. Res.*, *103*, 17,099–17,110.

Torres, O., P. K. Bhartia, J. R. Herman, A. Syniuk, P. Ginoux, and B. Holben (2002a), A long term record of aerosol optical depth from TOMS observations and comparison to AERONET measurements, *J. Atmos. Sci.*, *59*, 398–413.

Torres, O., R. Decae, J. P. Veefkind, and G. de Leeuw (2002b), OMI aerosol retrieval algorithm, in *OMI Algorithm Theoretical Basis Document: Clouds, Aerosols, and Surface UV Irradiance*, vol. 3, *version 2*, *OMI-ATBD-03*, edited by P. Stammes, pp. 47–71, NASA Goddard Space Flight Cent., Greenbelt, Md. (Available at http://eospso.gsfc.nasa.gov/eos_homepage/for_scientists/atbd/docs/OMI/ATBD-OMI-03.pdf)

Torres, O., P. K. Bhartia, A. Sinyuk, E. J. Welton, and B. Holben (2005), Total Ozone Mapping Spectrometer measurements of aerosol absorption from space: Comparison to SAFARI 2000 ground-based observations, *J. Geophys. Res.*, *110*, D10S18, doi:10.1029/2004JD004611.

Van Geffen, J., R. Van der A, M. Van Weele, M. Allaart, and H. Eskes (2004), Surface UV radiation monitoring based on GOME and SCIAMACHY, in *Proceedings of the ENVISAT & ERS Symposium, 6–10 September 2004, Salzburg, Austria*, *Eur. Space Agency Spec. Publ.*, *ESA SP-572*, Abstract 178.1.

Vaughan, M., S. Young, D. Winker, K. Powell, A. Omar, Z. Liu, Y. Hu, and C. Hostetler (2004), Fully automated analysis of space-based lidar data: An overview of the CALIPSO retrieval algorithms and data products, *Proc. SPIE Int. Soc. Opt. Eng.*, *5575*, 16–30.

Veefkind, J. P., and G. de Leeuw (1998), A new algorithm to determine the spectral aerosol optical depth from satellite radiometer measurements, *J. Aerosol Sci.*, *29*, 1237–1248.

Veefkind, J. P., J. F. de Haan, E. J. Brinksma, M. Kroon, and P. F. Levelt (2006), Total ozone from the Ozone Monitoring Instrument (OMI) using the DOAS technique, *IEEE Trans. Geosci. Remote Sens.*, *44*(5), 1239–1244.

Veihelmann, B., P. F. Levelt, P. Stammes, and J. P. Veefkind (2007), Simulation study of the aerosol information content in OMI spectral reflectance measurements, *Atmos. Chem. Phys.*, *7*, 3115–3127.

Verdebout, J. (2000), A method to generate surface UV radiation maps over Europe using GOME, Meteosat, and ancillary geophysical data, *J. Geophys. Res.*, *105*(D4), 5049–5058.

Welton, E. J., J. R. Campbell, J. D. Spinhirne, and V. S. Scott (2001), Global monitoring of clouds and aerosols using a network of micro-pulse lidar systems, *Proc. SPIE Int. Soc. Opt. Eng.*, *4153*, 151–158.

World Meteorological Organization (2007), Scientific assessment of ozone depletion: 2006, *Global Ozone Res. Monit. Proj. Rep. 47*, Geneva, Switzerland.

Zwally, H. J., et al. (2002), ICESAT's laser measurements of polar ice, atmosphere, ocean, and land, *J. Geodyn.*, *34*, 405–445.

C. Ahn, Science Systems and Applications, Inc., Lanham, MD 20706, USA.

P. K. Bhartia, NASA Goddard Space Flight Center, Greenbelt, MD 20771, USA.

R. Braak, P. Levelt, P. Veefkind, and B. Veihelmann, Netherlands Royal Meteorological Institute, NL-3730 AE De Bilt, Netherlands.

A. Tanskanen, Finnish Meteorological Institute, FIN-00101 Helsinki, Finland.

O. Torres, Joint Center for Earth Systems Technology, University of Maryland Baltimore County, Baltimore, MD 21250, USA.